

A Comparison of Measured and Simulated Air Pressure Conditions of a Detached House in a Cold Climate

Juha Jokisalo^{a,*}, Targo Kalamees^a, Jarek Kurnitski^a, Lari Eskola^a, Kai Jokiranta^a, and Juha Vinha^b

^aHVAC -Laboratory, Helsinki University of Technology, P.O. Box 4400, FIN-02015 TKK, Finland

^bInstitute of Structural Engineering, Tampere University of Technology, P.O. Box 600, 33101 Tampere, Finland

*Corresponding author. Tel.: +358-9-451-3598; fax: +358-9-451-3418
E-mail address: juha.jokisalo@tkk.fi

ABSTRACT

This study discusses the evaluation of a multi-zone infiltration model of an existing two-storey detached house in the cold Finnish climate. This study was performed by comparing the simulated and measured pressure conditions of the building during a three-week test period in the heating season. The simulations were carried out using a dynamic simulation tool, IDA-ICE, which combines whole-building energy simulation and infiltration modeling. The initial data for the building model were obtained with extensive field measurements, including measurements of the airtightness and air leakage distribution of the envelope and performance of the ventilation system. The study shows that the model is able realistically to predict the air pressure conditions of a detached house in a cold climate and it is suitable for detailed infiltration and energy analyses. The model allows the prediction of the effects of leakage distribution, airflows between rooms and floors, building leakage rate, pressure conditions, and climate on infiltration and energy use.

Keywords: airtightness; infiltration; air pressure conditions; leakage distribution; dynamic simulation; nodal network model

INTRODUCTION

Infiltration, defined as uncontrolled airflow through a building envelope, depends on the (average and local) air permeabilities of the building envelope and the air pressure difference between indoor and outdoor air across the building envelope. The pressure difference is caused by wind, the stack effect, and the ventilation system. Wind conditions are dependent on the building shape, size, location, degree of sheltering and other parameters in its surroundings. The stack effect depends on the height of the building and the temperature difference between indoor and outdoor air. The temperature differences of the air causes density differences that induce buoyancy force. The distribution of air leakage places and flow resistances between the rooms and floors

also have an effect on the stack-induced pressure difference over the local envelope. The stack effect is reversed in the cooling season but it is typically weaker in a cold climate as result of the smaller temperature difference between the inside and outside air. A mechanical supply and exhaust ventilation system induces negative or positive pressure differences in the building, depending on the ratio of the supply and return airflow rates. But, even if the total supply and return airflow rates are equal, the differences in design airflow rates for different room types (D2, 2003) induce pressure differences between the rooms, depending on air flow resistance on the path of air flow between the rooms.

Interzonal or multizone air flow models have been developed since the late '60s and their development was fast during the '70s and '80s. These models were used to simulate ventilation, infiltration, and indoor air quality in multizone buildings, taking account of air flows between the zones and through the building's envelope (Orme, 1999). Feustel and Dieris (1992) published an extensive literature review concerning 50 different multi-zone models developed during these decades. According to this study, fifteen of the simulation models allowed a combination of air flow simulation with a thermal simulation. In 2005 Crawley et al. made an extensive comparison between twenty major building energy simulation programs and reported only seven programs where multizone airflow simulation was available. Several studies have been carried out concerning different coupling methods of thermal and air flow models, for example, Clarke and Hensen (1990), Hensen (1995), and Sahlin (2003). Integration of the thermal and air flow models has been considered to be important, especially when coupling between heat and fluid flow is strong, for example with naturally ventilated buildings (Hensen, 1995), (Samuel, 2006). According to Sahlin (2003), buoyancy-driven interzonal air flows also have a significant impact on the heat balances of the rooms in airtight mechanically ventilated buildings.

The coupling of building energy simulation and CFD calculation has also been studied during recent years, for example by Negrao (1995), Beausoleil-Morrison (2000), Djunaery (2005), and Zhai and Chen (2005, 2006). In 2005 a study by Zhai and Chen indicated that the coupling of building energy simulation and CFD has marginal benefits for buildings with natural convection. In 2006 Zhai and Chen mentioned that this coupling is not necessary, for example, if the building has a fairly mixed indoor environment, the energy simulation tool used has properly calibrated heat transfer correlations, and indoor airflow is dominated by internal heat gains. But both of the preceding studies suggest that coupling should be used e.g. for buildings with major indoor air temperature stratification and/or considerable indoor air movement.

Scartezzini et al. (1987) and Feustel (1999) mention the difficulty of measuring infiltration in buildings under controlled boundary conditions and suspect that none of the multi-zone models have been validated properly, if at all. In this study, the simulated infiltration rate is not validated against the measurement result, but the comparison is made between simulated and measured air pressure conditions and the power law equation has been applied in the calculation of air flow through the leaks.

The objective of the study is to perform an evaluation of the air pressure conditions predicted by a detailed multi-zone simulation model which includes leakage distribution and other important parameters. A simulated distribution of leakage paths over the envelope is estimated with thermography tests estimating the location and size of the leakage paths by means of their impact on inside surface temperatures of the envelope. In addition, the use of simplified calculations of wind conditions and wind pressure coefficients available from the literature was evaluated.

METHODS

Building Description

The modeling object of the study is a detached house comprising two floors (Figure 1). The house is situated in the metropolitan area of Helsinki and was built in 2000. The net floor area of the house is 172 m². The structures of the house are a timber-frame construction insulated with mineral wool and provided with a plastic air vapor barrier. The base floor of the house is a concrete slab on the ground. The level of thermal insulation of the house fulfils the requirements of the Finnish building code (C3, 2003), which sets the target values for the thermal conductance of the building envelope: exterior walls $U \leq 0.25$ W/m² K, roof $U \leq 0.16$, W/m² K, the slab on the ground $U \leq 0.25$ W/m² K, and the windows $U \leq 1.4$ W/m² K. The house is equipped with a mechanical balanced (supply and exhaust) ventilation system and heated with an electrical floor heating system and ceiling-mounted radiant panels.



Figure 1. The object of the study is a typical Finnish detached house.

The method of construction, the ventilation system, and the tightness of the modeling object is similar to the typical detached house described in Vinha et al. (2005). The measured airtightness of the modeling object equals the mean level ($n_{50} = 3.9$ ach) of the 100 detached houses, that was measured in the preceding study.

Measurements

The initial data for the simulation model were collected by means of field measurements of the house. The following factors were measured:

- Ventilation at normal use of the air-handling unit
- Airtightness of the building envelope using a single pressurization test

- Air leakage distribution over all the facades and roof
- Air pressure difference over the building envelope (follow-up measurement during a three-week period)
- Indoor and outdoor temperature conditions (follow-up measurement during a three-week period).

The measurements of the ventilation air flow rates, airtightness, and air leakage distribution of the building envelope were carried out once (using a single-shot measurements). The supply and return air flow rates of each building zone (see Figures 2a, b) were measured from terminals at the low (3/8) speed of the air-handling unit, which is the normal use of ventilation in this studied house during the heating season. The resultant air change rate of the house was 0.3 ach and the input data of the simulation model concerning supply and return air flow rates are shown in Figure 2. For the sake of simplicity, some of the rooms were combined into one zone in the simulation model and the total measured air flow rates of the combined rooms were used in the simulations. The ventilation system is slightly negatively pressurized, because the ratio of the total supply and return air flow rates of the house was 0.94. The measured air change rate is lower than the minimum requirement of the Finnish building code (0.5 ach) (D2, 2003) and also slightly lower than the typical mean air change rate of detached houses (0.4 ach) in wintertime when equipped with a mechanical supply and exhaust ventilation system (Kurnitski et al. 2005).

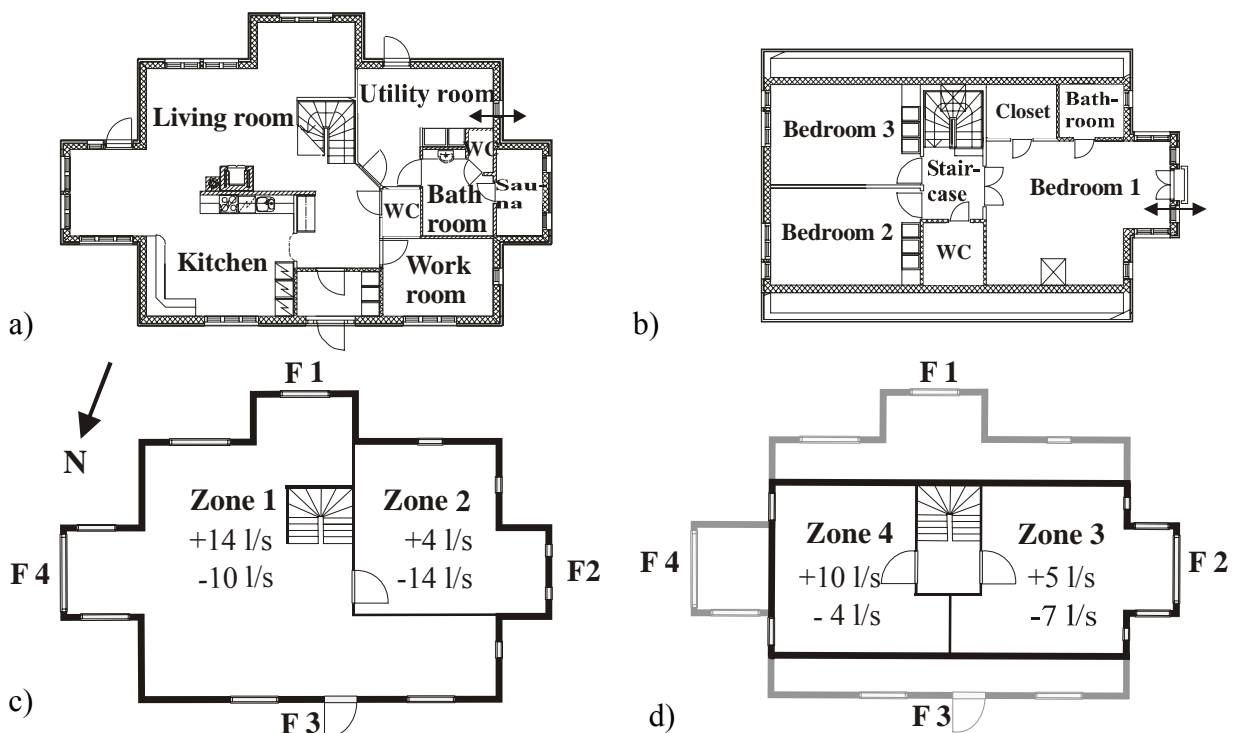


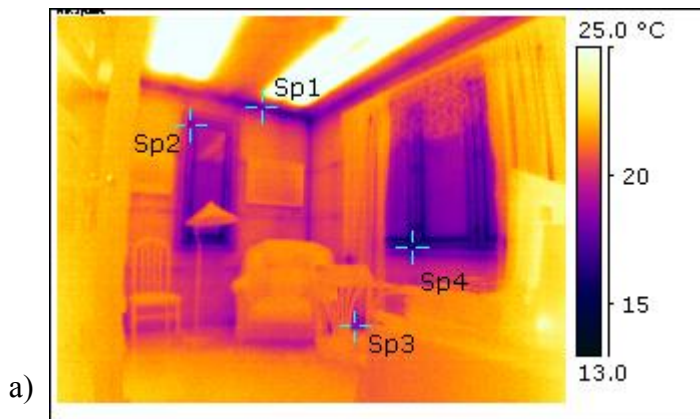
Figure 2. A plan of the base floor (a) and the top floor (b) of the simulated house and the floor plan of the simulation model (c and d). Supply air flow rates are shown with a (+) sign and return air flow rates with a (-) sign. The measurement points of the air pressure difference over the envelope are shown with arrows (a and b).

The airtightness of the building envelope was measured using a standardized (SFS-EN 13829, 2001) fan pressurization method. To measure the air leakage of the envelope depressurizing tests were conducted. All the exterior openings – windows and doors – were closed and the ventilation ducts and chimney were sealed. Measurements were made at 10 Pa pressure difference steps from 0 to 60 Pa. The leakage air change rate per hour at a pressure difference of 50 Pa was determined from the trend line of the measurement results. The leakage air flow rate was divided by the internal volume of the building to get the building leakage rate n_{50} ; the resultant figure was 3.9 ach. The air leakage rate of the building envelope equals the mean level of Finnish timber-frame detached houses: n_{50} : 3.9 ach. (Korpi et al. 2004).

To determine typical air leakage places and their distribution, a FLIR ThermaCam P65 infrared image camera (thermal sensitivity of 0.08 °C, measurement range -40 °C to +500 °C) and a smoke detector were used. Two thermography tests were performed during the winter period, when the difference between the indoor and outdoor temperatures was 25°C. All external walls and the roof were investigated from inside the house. Thermography investigations were performed once, to determine the normal situation, the surface temperature measurements were performed without any additional air pressure difference. Next, to determine the main air leakage places, a 50 Pa negative pressure over the envelope was set with fan pressurization equipment. After the infiltration airflow had cooled the inner surface (~30...45 min.) of the envelope, the surface temperatures were measured with the infrared image camera from the inside of the house. The temperature difference between these two measurements shows the air leakage path.

The relative decrease in the surface temperature was used to determine and to classify the air leakage places. The relative decrease in the surface temperature shows the relation of the temperature difference between the internal surface of the building envelope measured before ($T_{s,i1}$, °C) and after ($T_{s,i2}$, °C) the depressurization to the difference between the indoor (T_{in} , °C) and the outdoor (T_{out} , °C) air temperatures; see Equation 1.

$$\Delta T = \frac{T_{s,i1} - T_{s,i2}}{T_{in} - T_{out}} \times 100\% \quad (1)$$



Surface temperatures before the depressurization	
Point	$T_{s,i1}$, °C
Sp1	17.9
Sp2	17.9
Sp3	18.7
Sp4	15.3

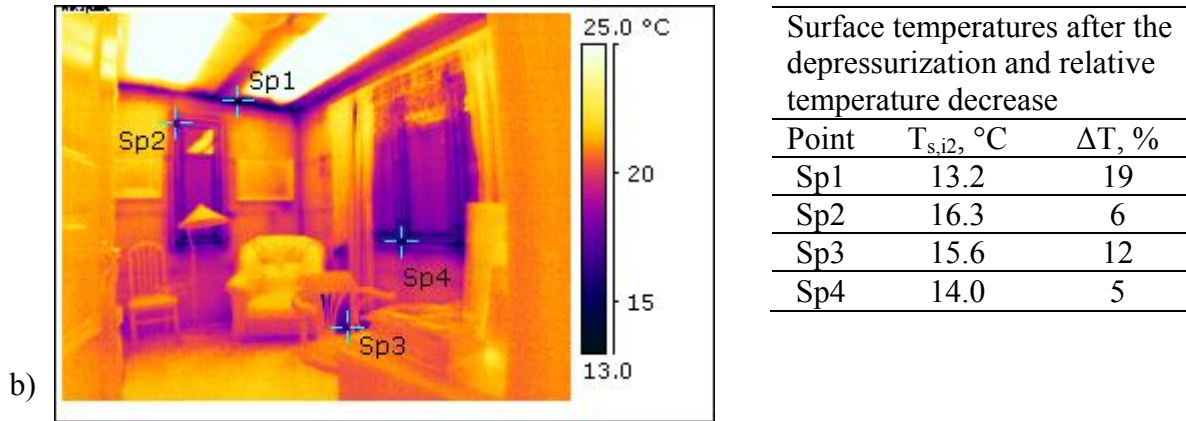


Figure 3. An example of infrared camera illustrations under normal (a) and -50 Pa pressure conditions (b).

Since our model (IDA-ICE) deals with a house as a system one needs to establish air leakage distribution over different locations. According to the air leakage distribution study of Finnish dwellings by Kalamees et al. (2007), typical air leakages were around and through windows and doors, in the junction of the ceiling/floor with the external wall, and penetrations through the air barrier systems. All these air leakage paths were also represented in the modeling object, while most significant air leakage paths were at a junction of the roof.

For the simulation model, the leakage paths of the modeling object were roughly classified according to the relative temperature decrease and the position. The shape or area of the leakage openings shown by the infrared camera illustrations are not taken into account, and nor are those leakage paths with a relative temperature decrease of less than 10%. The leakage paths that were taken into consideration were divided into three categories according to the relative temperature decrease ΔT ; see Table 1. The temperature decrease was simply taken into account using the assumed weighting factors f of the categories.

Table 1. Three categories of leakage paths based on the relative temperature decrease. The number x corresponds to the total number of leakage openings in the house that belong to these categories.

ΔT , %	Weighting factor f	Number x
10-20	1	33
20-30	2	18
>30%	3	5

Table 2. Typical vertical positions of the air leakage openings on both floors of the detached house that was studied.

Category Z	Typical place of the air leakage opening
1	Junction of external wall and roof
2	Upper edge of window frame
3	Lower edge of window frame
4	Junction of external wall and intermediate floor
5	Junction of external wall and base floor.

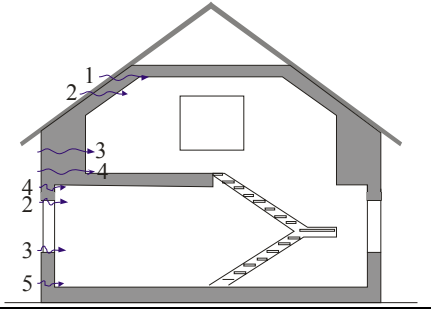


Table 2 shows five categories of air leakage path as seen from the inside surface of the envelope. While we do not know the actual leakage path from the entry to the exit we use the exit points and their impact as the distribution of the leakage on the entire facade. Effectively, a total of 23 leakage openings were modeled.

The product P of the weighting factor f and number x of the leakage paths was calculated for each facade F and category Z as follows:

$$P_{F,Z} = f_{F,Z} \cdot x_{F,Z} \quad (2)$$

The total sum of $P_{F,Z}$ in the house is calculated as the sum over all the facades F and the vertical positions Z.

$$P^{tot} = \sum_{F=1}^4 \sum_{Z=1}^5 P_{F,Z} \quad (3)$$

The distribution of the leakage openings in the house is approximated by dividing $P_{F,Z}$ by Equation (3) and the resultant leakage distribution is shown in Table 3.

$$D_{F,Z} = \frac{P_{F,Z}}{P^{tot}} \cdot 100\% \quad (4)$$

$D_{F,Z}$ is a proportion of a single leakage opening in the model to all the leakage openings taken into account. Since leakage paths are simulated with the power law equation, $D_{F,Z}$ shows a proportion of flow coefficient (see Equation 9) of single leakage path to the flow coefficient measured with whole building pressurization test.

Table 3. The leakage distribution of the house, based on the thermography investigation.

Place of the leakage paths			Leakage distribution of calculated zones, %				
Floor	Zone	Category Z	F 1	F 2	F 3	F 4	$\sum F$
top	3	1	7.1	13.1	1.2	0	21.4
		2	0	0	0	0	0
		3	0	1.2	1.2	0	2.4
		4	0	2.4	0	0	2.4
top	4	1	0	0	2.4	11.9	14.3
		2	0	0	0	3.6	3.6
		3	0	0	0	1.2	1.2
		4	0	0	0	0	0

base	1	4	2.4	1.2	3.6	8.3	15.5
		2	0	0	0	0	0
		3	2.4	1.2	4.8	2.4	10.8
		5	0	0	7.1	0	7.1
base	2	4	6.0	0	0	0	6.0
		2	0	0	0	0	0
		3	3.6	9.5	0	0	13.1
		5	0	2.4	0	0	2.4

The air pressure differences over the building envelope and room temperature of the building were measured during a three-week period in the heating season between 5th and 24th March 2005. Pressure differences were measured using calibrated FCO44 differential pressure transducers made by Furness Controls Ltd. The accuracy of these devices is better than $\pm 2.5\%$ in the measurement range from 0Pa to ± 20 Pa. Pressure difference data were collected with loggers using a 5-minute time step. The pressure difference was measured on the base and top floors of the building at the facade F2 (see Figures 2 and 4). Indoor air temperatures were measured in the living room on the base floor and in bedroom 1 on the top floor (see Figure 2) using Tinytag Plus loggers made by Gemini Data Loggers Ltd. The accuracy of this sensor is $\pm 0.2^\circ\text{C}$ in the range from 0°C to 50°C .

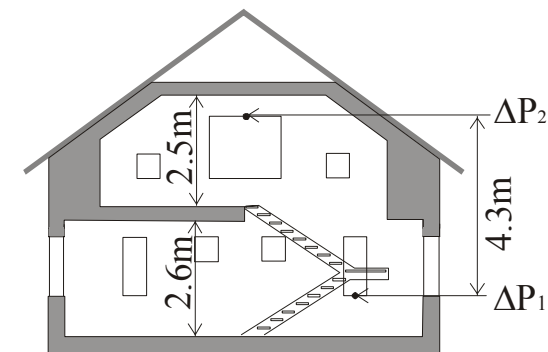


Figure 4. Measurement points of the air pressure difference over the building envelope at facade 2.

The occupants were living normally in this house during the follow-up measurements, which had an effect on the pressure and thermal conditions. The use of interior doors or other openings has a certain effect on the pressure conditions, but the indoor temperature is also linked to the pressure conditions by means of air density differences. Fluctuations in indoor temperatures depend on, for example, internal heat gains, which depend on the presence of the occupants and the use of devices and lighting. Furthermore, the use of curtains affects solar gains from the windows. It is not possible to get exact information about the behavior of the occupants. However, an enquiry concerning a typical way of living and use of equipment etc. during the test period was carried out and it was used as a basis for input data for the model.

The outdoor air temperature next to the detached house was also measured during the follow-up measurements. The measured outdoor air temperature and wind velocity at the closest weather station (distance from the detached house 30km) are shown in

Figure 5. The three-week period was cold; the average temperature was -7°C and the minimum temperature -18°C . The average wind velocity was 4.5m/s at the weather station, where the height of the measurement equipment from the ground is 10m and wind conditions are exposed. The local wind conditions of the detached house are simulated using a wind profile equation and terrain dependent coefficients shown in the next chapter.

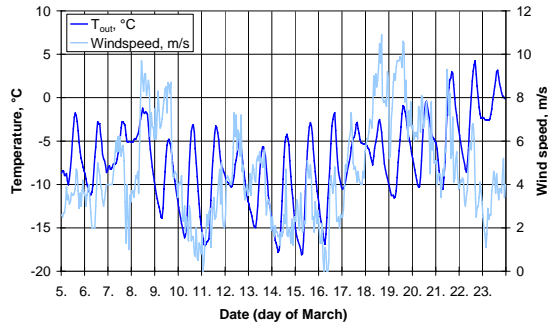


Figure 5. Measured outdoor temperature next to the detached house during follow-up measurements and the wind velocity measured at the weather station of the Finnish Meteorological Institute at the Helsinki-Vantaa airport.

The Dynamic Simulation

The building model was created using IDA indoor Climate and Energy 3.0 (IDA-ICE) building simulation software. This software allows the modeling of a multi-zone building, HVAC-systems, internal and solar loads, outdoor climate, etc. and provides dynamic simulation of heat transfer and air flows. It is a tool for the simulation of thermal comfort, indoor air quality, infiltration, and energy consumption in complex buildings. A modular simulation application, the IDA simulation environment and IDA-ICE, was originally developed by the Division of Building Services Engineering, Royal Institute of Technology (KTH), and the Swedish Institute of Applied Mathematics, ITM (Sahlin, 1996), (Björnsell et al. 1999), (Sahlin et al. 2004). Today the application is a commercial tool and IDA-ICE has reached high levels of penetration among practitioners and researchers in Sweden and Finland.

In the simulation model, the mass balance of air in each zone equals zero. Depending on the ratio of supply and return air flow rates in each zone, the air mass is balanced with air flows through the leaks in exterior walls or openings between zones, fulfilling the principle of mass conservation. The mass flows are simulated as a function of the air pressure difference between the zones and the outdoor environment. The building model of the detached house that was studied comprises two different zones on the base and top floors (see Figure 2); the floors are connected by means of a staircase. The air flow between the zones, the two floors, and outdoors caused by the pressure differences is simulated by means of the principle of a nodal network (see Figure 6), where the flow paths, cracks, or openings between the zones or outdoors are described as flow resistances.

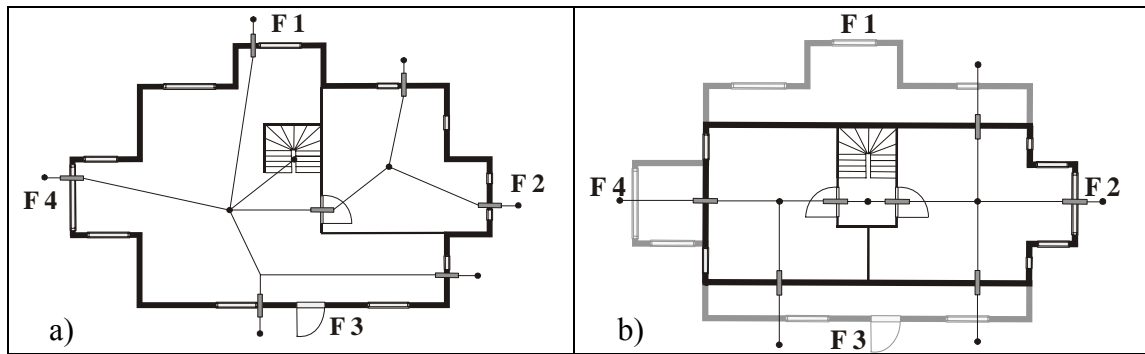


Figure 6. A top view of the nodal network model of the base (a) and the top (b) floors. Gray boxes show the flow resistances of the flow paths; the pressures are calculated at the black nodes.

In the air handling unit model of the detached house, the fans have ideal pressure control with fixed pressure heads. Basically, supply and exhaust fans transfer a constant air mass flow in and out of the zones when the air handling unit operates in a constant air volume (CAV) mode. This air handling unit (see Figure 7) is equipped with heat recovery via a recuperative plate heat exchanger with a 60% temperature efficiency. The air handling unit is provided with defrost protection of the heat exchanger. In this air handling unit, the defrost protection is controlled so that the minimum achievable exhaust temperature after the heat exchanger is $+4^{\circ}\text{C}$. When the exhaust air temperature falls below $+4^{\circ}\text{C}$, the supply fan is turned off. This feature was included in the model because the simulation period describes the cold season when defrost protection is normally needed. Because exact information about the operating time of the supply fan of the modeling object was not available, the control of the defrost protection in the model was based on the simulated return air flow temperature after heat recovery. The other possible solutions for defrost protection are not based on the stopping of the supply fan, but, for example, on bypassing the supply air with dampers (Nyman, 1987). The effect of these two defrost protection methods on the pressure conditions of the building is studied with two separate cases.

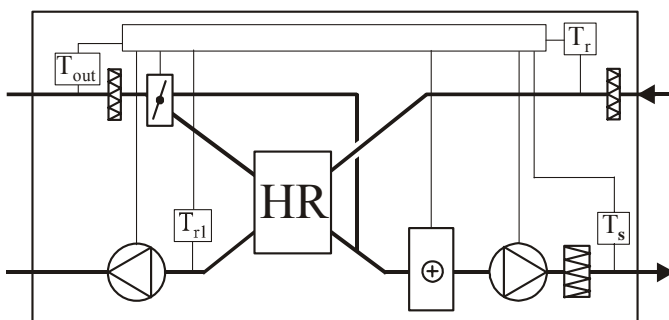


Figure 7. The principle of the air handling unit in the mechanical supply and exhaust ventilation system. T_{out} refers to the outdoor air temperature, T_r to the return air temperature, T_{r1} to the return air temperature after the heat exchanger, and T_s to the supply air temperature.

Wind pressure distribution around the house is simulated using the normal assumption in building engineering that the wind flow is horizontal and an atmospheric boundary layer is neutral without vertical air flow. The wind conditions of the environment were approximated using the wind profile equation reported in ASHRAE Fundamentals (1989); see Equation 5. This profile basically corresponds to the LBL model wind profile (Sherman and Grimsrud, 1980).

$$U(h) = U_m \cdot k \cdot \left(\frac{h}{h_m} \right)^a \quad (5)$$

where $U(h)$ is the wind speed at height h (m/s), U_m is the wind speed measured in open country at the weather station (m/s), h is the height from the surface of the ground (m), h_m is the height of the measurement equipment (10 m), and parameters k and a are terrain-dependent constants. The simulated building is located in a typical Finnish suburban area with closely built houses where the height of adjacent houses is approximately the same as the simulated one. The wind profile equation was simulated using values for terrain parameters k (0.67) and a (0.25) that correspond to the values of the standard urban area terrain class published by Sherman and Grimsrud (1980).

The wind profile (Equation 5) with given terrain parameters predicts undisturbed wind approaching a building. The wind profile equation is less reliable below a certain height, which is related to the average height of the buildings and vegetation in the surroundings, because wind speed and direction depend on the geometrical arrangement of the obstacles. The layer below which wind profile equations are not valid is sometimes referred to as an urban canopy. For example, Hensen (1991) gave a relation between the height of the urban canopy, terrain roughness, and building height. In practice, this is roughly compensated by calculating wind-induced pressure conditions at the height of the exterior wall using wind pressure coefficients that describe the local shielding. It is evident that wind pressure coefficients should be defined via wind tunnel experiments or CFD calculations that take individual obstacles in the surroundings into account.

However, in this study, the calculation of wind conditions was simplified and wind pressure coefficients were not measured nor simulated, but wind coefficient data available from the literature were utilized. One object of this study was to evaluate the applicability of this simplification; is it possible to predict realistic pressure conditions of this detached house using that assumption? The values of the wind pressure coefficients used in this study were presented by Liddament (1986) (see Table 4). These wind pressure coefficients are approximated values for low-rise buildings surrounded on all sides by obstacles equal to the height and size of the house. These data were originally produced in two wind tunnel scale model experiments published by Bowen in 1976 and Wiren in 1985. Bowen studied local wind pressure coefficients for a 2:1 rectangularly shaped building scale model surrounded by obstructions of varying size and Wiren studied 1½-storey detached houses with a pitched roof with various surrounding building densities. As shown in Figure 2, the shape of the building being studied is more complicated than that of a simple rectangular building, so the simulated wind pressure distribution around the building was also considerably simplified in this

respect. Additionally, the pitched roof of the modeling object was simplified to become a flat roof in the simulation model.

Table 4. Wind pressure coefficient of a detached house. The wind angle 0° corresponds to wind flowing from the south.

Wind Angle,°	Facade			
	F 1	F 2	F 3	F 4
0	0.06	-0.3	-0.3	-0.3
45	-0.12	0.15	-0.38	-0.32
90	-0.2	0.18	-0.2	-0.2
135	-0.38	0.15	-0.12	-0.32
180	-0.3	-0.3	0.06	-0.3
225	-0.38	-0.32	-0.12	0.15
270	-0.2	-0.2	-0.2	0.18
315	-0.12	-0.32	-0.38	0.15

The wind pressure outside the building facades P_w is determined by Equation (6)

$$P_w = C_p \cdot \frac{1}{2} \rho_{out} \cdot U^2 \quad (6)$$

where ρ_{out} is the outdoor air density (kg/m^3), C_p is the wind pressure coefficient, and U is the local wind velocity defined by Equation (5). Because of the square dependence of the wind velocity in Equation (6), wind velocity has a more significant effect on wind pressure than the value of the wind pressure coefficient. The local outside surface pressure P_s on the building facades follows the equation

$$P_s = P_{out} - \rho_{out} \cdot g \cdot h + P_w \quad (7)$$

where P_{out} is the outdoor air pressure at ground level (Pa), ρ_{out} is the outdoor air density (kg/m^3), and g is the acceleration of gravity (m/s^2). The pressure difference between the zone and outdoor air is calculated as

$$\Delta P = P_{in} - \rho_{in} \cdot g \cdot h_{in} - P_s \quad (8)$$

where P_{in} is the indoor air pressure at floor level (Pa), ρ_{in} is the indoor air density (kg/m^3), and h_{in} is the height from floor level (m). The air densities shown in Equations (7) and (8) are calculated as a function of temperature and moisture using ideal gas laws coded in the ASHRAE secondary toolkit models (1993). This driving pressure difference of infiltration shown in Equation (8) is calculated for every air leakage opening in the model, combining the effect of mechanical ventilation, wind, and stack effect. The air leakage openings were distributed over the building model according to the measured leakage distribution shown in Table 3.

The air flow through a leakage opening Q is simulated in the building model with the empirical power law equation. This equation is widely accepted in measurements and air infiltration standards (Liddament, 1987), (Walker, 1998), while Sherman (1992) has developed theoretical basis of this expression. The power-law equation is commonly

used in multizone models (Feustel, 1992) and a validity of this kind of approach is studied, for example, (Blomsterberg et al. 1999). IDA-ICE uses a linearized power law equation around a zero pressure difference resulting from numerical reasons and normal power law equation when the pressure difference equals or exceeds a limit value of linearization dp_0 (Sahlin, 1996).

$$Q = \begin{cases} C_0 \cdot \Delta P, & |\Delta P| < dp_0 \\ \pm C |\Delta P|^n, & |\Delta P| \geq dp_0 \end{cases} \quad (9)$$

where C_0 is a linearized flow coefficient, C is a flow coefficient that is related to the size of the opening, ΔP is the pressure difference across the opening defined by Equation (8), and n is a flow exponent characterizing the flow regime. A plus-minus sign in the equation means that the flow is bi-directional; when ΔP is negative, the mass flow is considered to be inflow. The flow exponent in the power law equation varies in value from 0.5 for a fully turbulent flow to 1.0 for a completely laminar flow. A typical value for the flow exponent suggested by Orme et al. (1998) is 0.66, based on extensive field measurements carried out in five countries. Based on the pressurization tests of 100 Finnish timber-frame detached houses, the average flow exponent of all the houses was 0.72 and the resultant value of this modeling object was 0.63. The leakage air flow Q (kg/s) measured in the pressurization test is shown as a function of the building leakage number n_{50} (ach)

$$Q = \frac{\rho_{out} \cdot n_{50} \cdot V_{building}}{3600} \quad (10)$$

where $V_{building}$ is the internal volume of the building (m^3) and 3600 is a conversion factor from hours to seconds. Substituting Equation (10) into the nonlinearized power law equation (9), the flow coefficient of the modeling object can be calculated and the resultant value for the measured detached house is $(0.0486 \text{ kg/s, Pa}^n)$. The linearized flow coefficient is defined as

$$C_0 = C \cdot dp_0^{n-1} \quad (11)$$

The default limit value for linearization (dp_0) is 5Pa in IDA-ICE 3.0, but this model was simulated using 0.1Pa as the limit. Additionally, Walker et al. (1998) found a slight trend for the crack flow to be laminar below a pressure difference of 0.1 Pa. As an example, mass flows calculated using both linearized and nonlinearized power law equations are shown in Figure 8. In practice, the effect of linearization on mass flow is negligible with a 0.1 Pa limit, because the absolute pressure difference value over the envelope usually exceeds 0.1Pa in these kinds of detached houses (Kalamees et al. 2007).

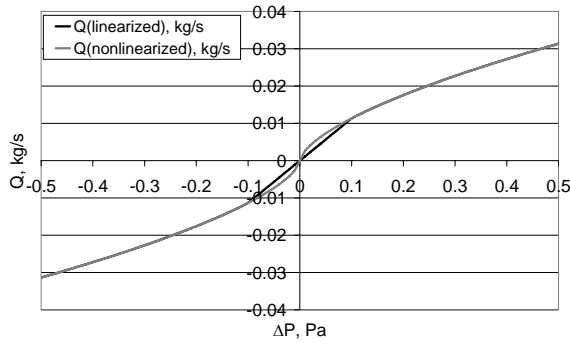


Figure 8. Infiltration air flow calculated with linearized and nonlinearized power law equations.

In the model, small openings or cracks between the zones are simulated using power law equation (9), but large vertical openings such as an open door between the zones are simulated with the model reported by Bring et al. (1999). There, the vertical flow profile in the opening depends on the density differences between the adjoining zones; if the densities are equal, the flow profile is flat; otherwise it is slanted. In the case of a flat velocity profile, the air mass flow between the zones is calculated with the standard orifice flow equation

$$Q = C_d \cdot A \sqrt{2\rho \cdot \Delta P} \quad (12)$$

where C_d is a discharge coefficient and A is the area of the opening (m^2). In the case of a slanted profile, the air flow between the zones is simultaneously bi-directional (Bring et al. 1999).

RESULTS

The results of the three-week empirical validation period are presented and discussed below. The building model was simulated using the hourly weather data of the three-week measurement period. The local measured outdoor temperature data were used and the other data required, for example, the wind velocity and direction and solar radiation properties, were taken from the closest weather station. The simulated air pressure difference over the building envelope on the base and top floors of the detached house and the average indoor air temperatures are compared against the measurement results. The simulated pressure differences were logged from the building model at the same facade and at the same height from the ground as in the measurements. Two different cases are simulated concerning the methods of defrost protection of the heat recovery system in the air handling unit:

- Case 1: On/off control of the supply fan, as it is in the measured house.
- Case 2: Bypass control of the supply fan.

The measured and simulated average indoor air temperatures and pressure differences during the test period are shown in Table 5. The differences in the average indoor air temperatures between the measurement and simulation results are insignificant when the measurement accuracy of $\pm 0.2^\circ\text{C}$ is taken into account. The indoor air temperatures of

the building are rather low, especially on the top floor, because of the occupants' way of life. The average air pressure differences are slightly negative on the base floor and positive on the top floor. The differences between the average measured and simulated pressure differences are quite small; the maximum error is 0.6Pa in case 1 and 1.1Pa in case 2. The accuracy of the pressure probes is better than $\pm 0.08\text{Pa}$ in this pressure range.

Table 5. Measured and simulated average indoor air temperatures and pressure differences over the envelope during the three-week test period.

Method	Indoor air temperature, °C		Pressure difference, Pa	
	1 st floor	2 nd floor	1 st floor	2 nd floor
Measurement	19.7	17.0	-3.3	1.9
Simulation-case 1	19.7	17.2	-2.7	2.2
Simulation-case 2	19.8	17.2	-2.2	2.8

Figure 9 shows the measured and simulated hourly air pressure differences over the envelope. In both simulation cases, the model gives some peaks that clearly deviate from the measured pressure. For example, the measured peaks of pressure differences were positive on the top and base floors on 17th March, but the model gave opposite (negative) pressure differences (see Figures 9a, b). It is probable that these kinds of errors result from the simplifications made in the calculation of wind pressure. In case 1, the simulated pressure differences follow the measurement results more precisely and the correspondence between the results is quite good, while the model tends to overestimate the pressure differences more in case 2.

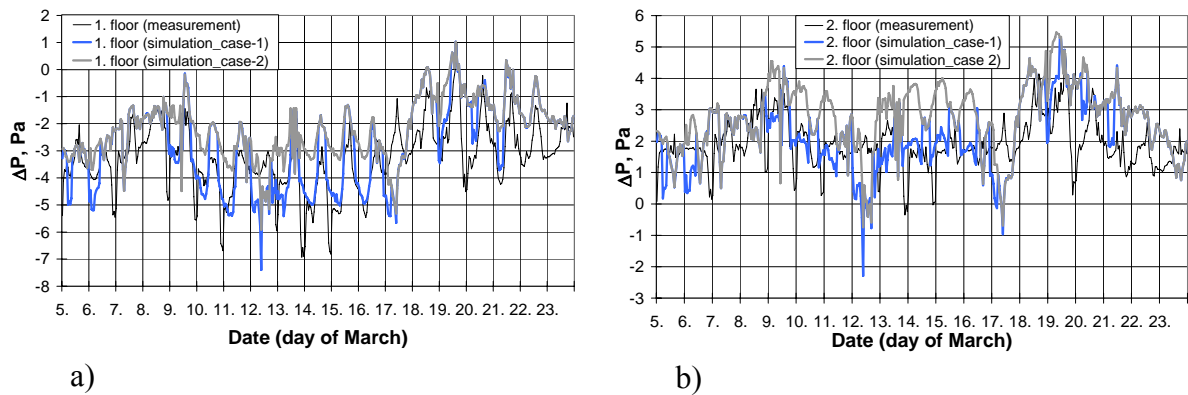


Figure 9. Measured and simulated air pressure conditions of the detached house on the base (a) and top (b) floors during the three-week measurement period from 5th to 24th March 2005.

In Figure 10, the air pressure differences are shown as a function of the temperature difference between indoor and outdoor air. According to the measurement results (see Figure 10), the pressure difference decreases with an increasing temperature difference on the base floor, but the temperature dependence of the pressure difference is weak on the top floor. The different measured correlations between the air pressure and the temperature differences on the base and top floors are the result of different factors, such as the stack effect and the method of defrost protection. Results show that this can be simulated more accurately in case 1, where the defrost protection method of the modeling object is taken into account (see Figures 10a, c). In case 2, where the fans of

the air handling unit are always on (see Figures 10b, d), the model predicts somewhat higher pressure differences than the measurement result at the lowest outdoor air temperatures.

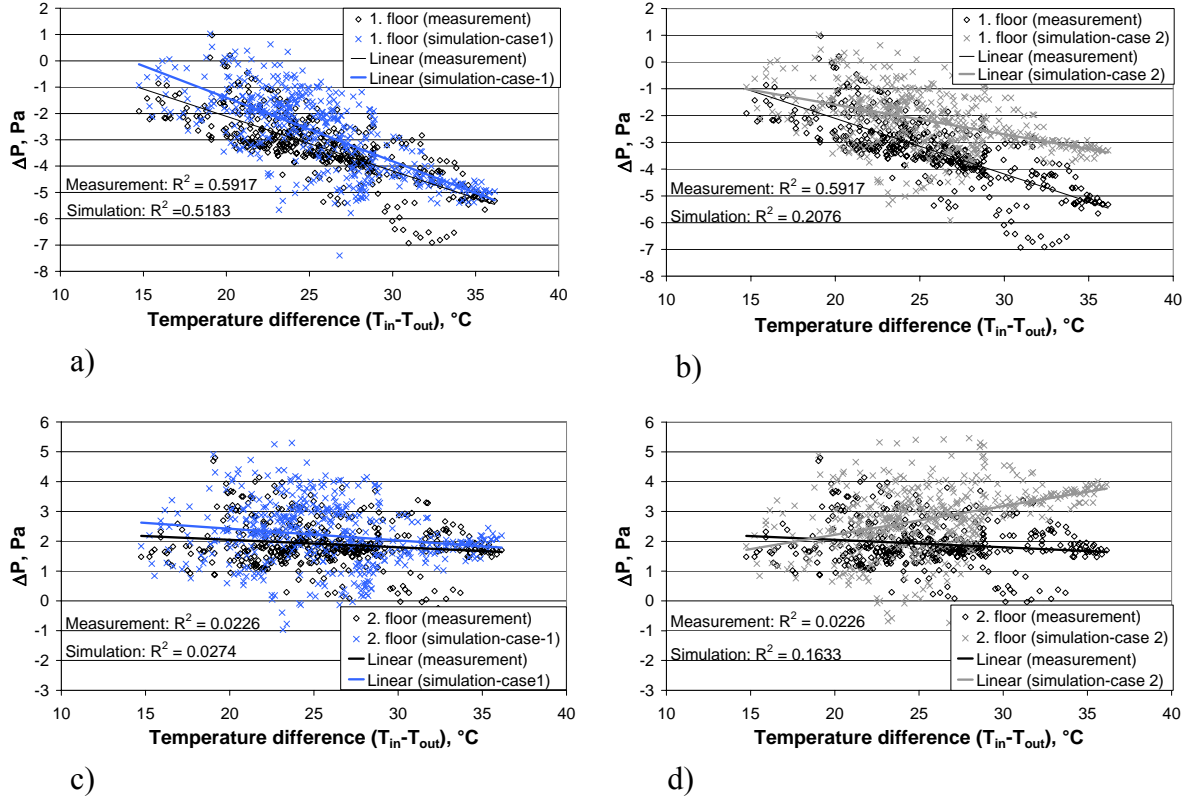


Figure 10. Measured and simulated pressure conditions of the detached house on the base (a, b) and top (c, d) floors during the test period. The pressure differences are shown as a function of the temperature difference between indoors and outdoors.

The error, defined as the difference between the measured and simulated air pressure differences (case 1) over the envelope on the top floor, is shown as a function of local wind speed and direction (see Figure 11). In Figure (11a) the local wind speed at the level of the roof of the detached house is approximated with Equation (5) and the wind direction is the measurement result from the weather station in Figure (11b). According to Figure (11a), this error between the measured and simulated air pressure differences does not depend on the wind speed. It is not possible to get a true correlation between the error and all wind directions, because Northerly wind directions predominated during the cold test period (see Figure 11b). But the mean absolute values of the error between the compass points give an indication that the error does not depend strongly on the wind direction. It seems that the simplified assumptions made with a simulation of wind pressure are suitable for this detached house.

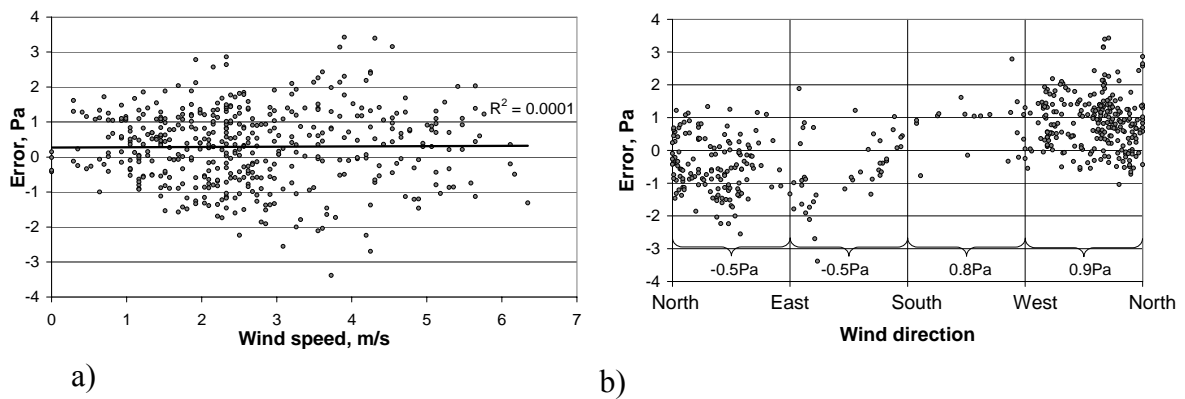


Figure 11. The errors between the simulated (case 1) and measured air pressure differences over the envelope on the top floor. The errors are shown as a function of wind speed (a) and direction (b). The average errors between the main compass points are also shown in Figure (b).

The measured and simulated air pressure differences between the top and the base floors are shown in Figure 12. This air pressure difference is mainly because of the stack effect (Kalamees et al. 2007) and the correspondence between the results is good. The simulation result corresponds to case 1, but the difference between the simulation cases is insignificant in this respect.

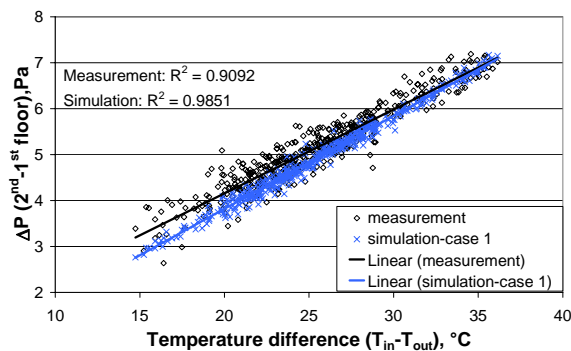


Figure 12. Measured and simulated air pressure differences between the top and the base floors during the measurement period. The pressure difference over the envelope on the top floor is subtracted by the corresponding pressure difference on the base floor.

APPLICATION

The applicability of this simulation model was studied with a simulation of the modeling object over a period of one whole year. The simulation was carried out with the hourly weather data for Helsinki 1979, which are commonly used as test reference data for energy calculations in Finland (Tammelin and Erkiö, 1987). Figure 13 shows the hourly infiltration air change rate and pressure conditions of this detached house over the whole simulation period. According to the example, the infiltration air flow clearly increases during the heating season in a cold climate, while the average annual infiltration rate is 0.19 ach. In this example, the top floor air pressure is positive for more than 90% of the year, with a maximum pressure of approximately 6Pa. Long-term

positive pressure should be taken into account in design in order to achieve a moisture-safe building envelope, because exfiltration may cause a significant moisture load to enter into the building envelope.

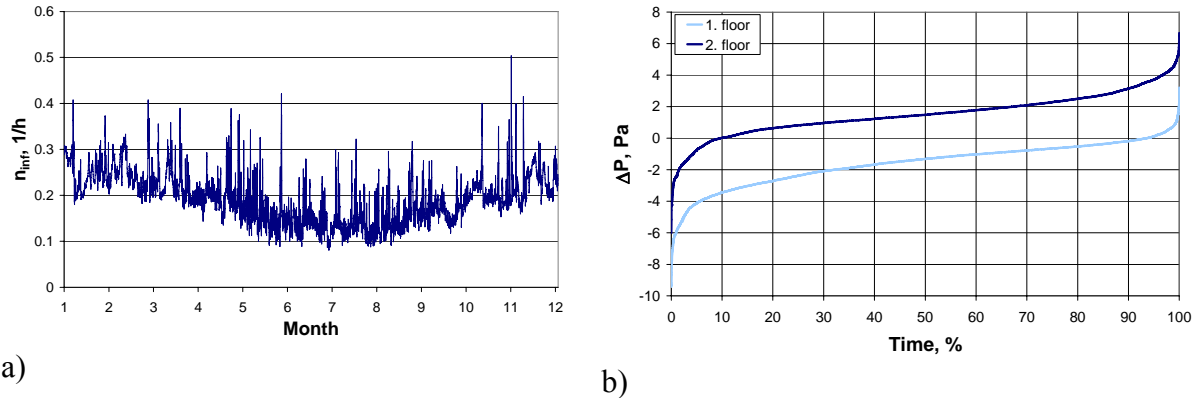


Figure 13. Simulated infiltration air change rate of the detached house (a) and duration curve of air pressure difference over the envelope (b) on the base and the top floors.

The effect of the building leakage rate on heat energy consumption is studied by also simulating the modeling object with $n_{50} = 0.15$ ach, which corresponds to an almost completely airtight building. This difference in the building leakage rate reduces the heat energy consumption of the zones and the ventilation system by $25\text{kWh/m}^2\text{,a}$, when the infiltration heat recovery effect (Virtanen, 1993) is not taken into account. This result indicates that in the detached house that was studied, about 30% of the heat energy consumption regarding the zones and ventilation is caused by infiltration. If the preceding heat recovery effect was taken into account, the energy impact of infiltration would be slightly lower.

CONCLUSIONS

This evaluation exercise shows that the dynamic multi-zone simulation model that was studied, with specific features such as detailed leakage distribution and defrost protection of heat recovery, predicts the air pressure conditions of a detached house in sheltered wind conditions and a cold climate realistically. The simulated air pressure conditions of the building model are reasonable, even if the calculation of the wind-induced pressure conditions was greatly simplified, for example with approximate wind pressure coefficients and wind data that were taken from the closest airport's weather station. This study was carried out for the cold period of the winter season when the buoyancy-driven pressure difference was emphasized and the building being studied was situated in a sheltered suburban area. This reduces the effect of the wind on pressure conditions in the detached house. Another reason why the winter was selected for the analysis period is that during a cold period moisture convection resulting from positive air pressure clearly raises the moisture accumulation rate in the building envelope. The study shows that this multi-zone model can be used for infiltration and energy analyses in the cold Finnish climate.

ACKNOWLEDGEMENTS

This study was supported by a grant from the Finnish Academy (Grant 210683). The study utilizes the measuring data of the national research project “Air tightness, indoor climate and energy efficiency of residential buildings”, which was carried out by the Laboratory of Structural Engineering at Tampere University of Technology and the HVAC Laboratory at Helsinki University of Technology. The financial support of the National Technology Agency of Finland, TEKES, and Finnish companies and associations participating in the project is gratefully acknowledged.

REFERENCES

- ASHRAE Handbook Fundamentals. (1989). American Society of Heating, Refrigerating and Air Conditioning Engineers, Atlanta.
- ASHRAE HVAC Secondary Toolkit. (1993). A toolkit for secondary HVAC systems energy calculations, American Society of Heating, Refrigerating and Air Conditioning Engineers, Atlanta.
- Beausoleil-Morrison, I. (2000). *Adaptive coupling of heat and air flow modeling within dynamic whole building simulation*, PhD Thesis, Energy System Research Unit, Department of Mechanical Engineering, University of Strathclyde, Glasgow, UK.
- Björzell, N., Bring, A., Eriksson, L., Grozman, P., Lindgren, M., Sahlin, P. and Shapovalov, A. (1999). IDA indoor climate and energy, Proceedings of the IBPSA Building Simulation '99 conference. Kyoto, Japan.
- Blomsterberg, Å., Carlsson, T., Svensson, C. and Kronvall, J. (1999). Air flows in dwellings – simulations and measurements, *Energy and Buildings*, **30**(1): pp. 87-95.
- Bowen, A. J. (1976). A wind tunnel investigation using simple building models to obtain mean surface wind pressure coefficients for air infiltration estimates, National aeronautical establishment, National Research Council Canada, report LTR-LA-209.
- Bring, A., Sahlin, P. and Vuolle, M. (1999). Models for Building Indoor Climate and Energy Simulation, Report of IEA SHC Task 22, Subtask B, Model documentation.
- C3. (2003). *Thermal insulation in a building*, The National Building Code of Finland, part C3.
- Clarke, J. A. and Hensen, J. (1990). An approach to the simulation of coupled heat and mass flow in buildings. In: *Proceedings of the 11th AIVC Conference*, September 18-21 1990, Belgirate, Italy, Vol 2. pp. 339-354.
- Crawley, D. B., Hand, J. W., Kummert, M. and Griffith, B. T. (2005). Contrasting the capabilities of building energy performance simulation programs. In: *Proceedings of Building Simulation 2005*, 15-18 August 2005, Montreal, Quebec, Canada. IBPSA.
- D2. (2003). *Indoor Climate and Ventilation of Buildings*. The National Building Code of Finland, part D2.
- Djunaery, E. (2005). *External coupling between building energy simulation and computational fluid dynamics*, PhD Thesis, Eindhoven University of Technology, Eindhoven, Netherlands.
- Feustel, H. E. and Dieris, J. (1992). A survey of airflow models for multizone structures, *Energy and Buildings*, **18**(2): pp. 79-100.
- Feustel, H. E. (1999). COMIS – an international multizone air-flow and contaminant transport model, *Energy and Buildings*, **30**(2): pp. 3-18.
- Hensen, J. (1991). *On the thermal interaction of building structure and heating and ventilating system*, PhD Thesis, Eindhoven University of Technology, Eindhoven, Netherlands.
- Hensen, J. (1995). Modelling coupled heat and air flow: Ping-pong vs. onion. In: *Proceedings of the 16th AIVC Conference*, 19-22 September, 1995, Palm Springs, USA, Vol. 1, pp. 253-262.

- Kalamees, T., Kurnitski, J., Korpi, M. and Vinha, J. (2007). The distribution of the air leakage places and thermal bridges of different types of detached houses and apartment buildings. In: *Proceedings of the 2nd European Blower Door Symposium*, Kassel, Germany, March 16 and 17, 2007.
- Kalamees, T., Kurnitski, J., Jokisalo, J., Eskola, L., Jokiranta, K. and Vinha, J. (2007). Air pressure conditions in Finnish residences. In: *Proceedings of the 9th REHVA World Congress - Clima 2007*, Helsinki, Finland, 10.06.2007-14.06.2007.
- Korpi, M., Vinha, J. and Kurmitski, J. (2004). Air tightness of timber-framed houses with different structural solutions. In: *Proceedings of the 9th international conference - Performance of exterior envelopes of whole buildings*, December 5-10 2004, Florida.
- Kurnitski, J., Eskola, L. and Palonen, J. (2005). Ventilation in 102 Finnish single-family houses, *Proceedings of the 8th REHVA World Congress - Clima 2005*, Lausanne, Switzerland, 9-12 October 2005. CD-Rom. 7 p.
- Liddament, M. (1986). Air infiltration calculation techniques – an application guide, *Air Infiltration and Ventilation Centre*, UK.
- Liddament, M. W. (1987). Power law rules – OK? *Air Infiltration review*, **8**(2):pp. 4-6.
- Negrao, C. O. R. (1995). *Conflation of computational fluid dynamics and building thermal simulation*, PhD Thesis, Energy System Research Unit, Department of Mechanical Engineering, University of Strathclyde, Glasgow, UK.
- Nyman, M. (1987). Ilmanvaihdon lämmöntalteenottolaitteiden jäätyminen (Freezing of ventilation heat recovery systems), VTT Technical Research Centre of Finland, HVAC-laboratory, Espoo. (in Finnish).
- Orme, M., Liddament, M. and Wilson, A. (1998). Numerical data for air infiltration & natural ventilation calculations, Technical note 44, Air Infiltration and Ventilation Centre, UK.
- Orme, M. (1999). *Applicable models for air infiltration and ventilation calculations*, Technical note 51, Air Infiltration and Ventilation Centre, UK.
- Sahlin, P. (1996). *Modelling and simulation methods for modular continuous system in buildings*. PhD Thesis. Royal Institute of Technology (KTH), Stockholm, Sweden.
- Sahlin, P. (2003). On the effects of decoupling air flow and heat balance in building simulation models, *ASHRAE Transactions*, **109**(2): pp. 788- 800.
- Sahlin, P., Eriksson, L., Grozman, P., Johnsson, H., Shapovalov, A. and Vuolle, M. (2004). Whole-building simulation with symbolic DAE equations and general purpose solvers. *Building and Environment*, **39**(8): pp. 949-958.
- Samuel, A. A. (2006). *On the conflation of contaminant behaviour prediction within whole building performance simulation*, PhD Thesis, Energy System Research Unit, Department of Mechanical Engineering, University of Strathclyde, Glasgow, UK.
- Scartezzini, J., Furbringer, J., Roulet, C. and Feustel, H. (1987). Data needs for purpose of air infiltration computer code validation. In: *Proceedings of the 8th AICV Conference*, Ventilation Technology – Research and application, 21-24 September 1987, Überlingen, West Germany, pp 7.1-7.18.
- SFS-EN 13829. (2001). Thermal performance of buildings - determination of air permeability of buildings - fan pressurization method, Finnish Centre for Standardization.
- Sherman, M. and Grimsrud, D. (1980). Infiltration - pressurization correlation: Simplified physical modeling. *ASHRAE Transactions*, vol. 86, part 2. pp. 778-807.
- Sherman, M. (1992). A power law formulation of laminar flow in short pipes, *Journal of Fluids Engineering*, **114**(4): pp. 601-605.
- Tammelin, B. and Erkiö, E. (1987). Energialaskennan säätiedot – suomalainen testivuosi (Weather data for energy calculation – The Finnish test year), Finnish Meteorological Institute, Weather department – Technical climatology, Report 7, Helsinki, Finland. (in Finnish)
- Vinha, J., Korpi, M., Kalamees, T., Eskola, L., Palonen, J., Kurnitski, J., Valovirta, I., Mikkilä, A. and Jokisalo, J. (2005). Puurunkoisten pientalojen kosteus- ja lämpötilaolosuhteet,

- ilmanvaihto ja ilmatiiviyys (Indoor temperature and humidity conditions, ventilation and air tightness of Finnish timber-framed detached houses), Research report 131, Structural Engineering laboratory, Tampere University of Technology, Finland. (in Finnish).
- Virtanen, M. (1993). *Thermal coupling of leakage air and heat flows in buildings and in building components*, PhD Thesis, VTT Technical Research Centre of Finland, HVAC-laboratory, Espoo, Finland.
- Walker, I., Wilson, D., Sherman, M. (1998). A comparison of the power law to quadratic formulations for air infiltration calculations, *Energy and Buildings*, **27**(3): pp. 293-299.
- Wiren, B. (1985). Effects of surrounding buildings on wind pressure distributions and ventilation losses for single-family houses, Part 1: 1 ½-storey detached houses, The Swedish National Institute for Building Research, Sweden.
- Zhai, Z. and Chen, Q. (2005). Performance of coupled building energy and CFD simulations, *Energy and Buildings*, **37**(4): pp. 333-344.
- Zhai, Z. and Chen, Q. (2006). Sensitivity analysis and application guides for integrated building energy and CDF simulation, *Energy and Buildings*, **38**(9): pp. 1060-1068.